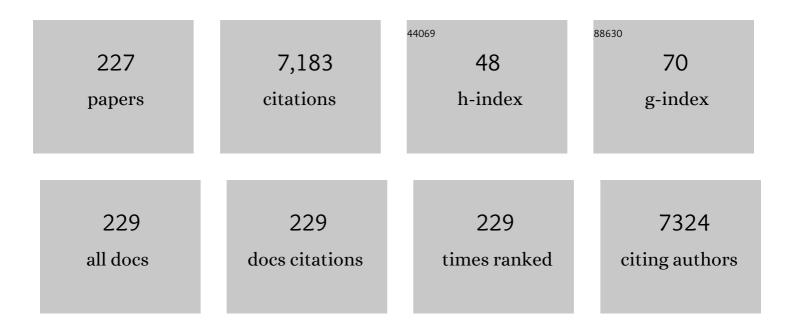
Shengping Ruan

List of Publications by Year in descending order

Source: https://exaly.com/author-pdf/920670/publications.pdf Version: 2024-02-01



#	Article	IF	CITATIONS
1	Role of tungsten oxide in inverted polymer solar cells. Applied Physics Letters, 2009, 94, .	3.3	294
2	Performance improvement of inverted polymer solar cells with different top electrodes by introducing a MoO3 buffer layer. Applied Physics Letters, 2008, 93, .	3.3	211
3	Enhanced H2S sensing characteristics of CuO-NiO core-shell microspheres sensors. Sensors and Actuators B: Chemical, 2015, 209, 515-523.	7.8	177
4	TiO2 based metal-semiconductor-metal ultraviolet photodetectors. Applied Physics Letters, 2007, 90, 201118.	3.3	170
5	Microwave absorptive behavior of ZnCo-substituted W-type Ba hexaferrite nanocrystalline composite material. Journal of Magnetism and Magnetic Materials, 2000, 212, 175-177.	2.3	162
6	Metal-semiconductor-metal TiO2 ultraviolet detectors with Ni electrodes. Applied Physics Letters, 2009, 94, .	3.3	140
7	On the high response towards TEA of gas sensors based on Ag-loaded 3D porous ZnO microspheres. Sensors and Actuators B: Chemical, 2018, 270, 492-499.	7.8	124
8	Xylene gas sensor based on Au-loaded WO3·H2O nanocubes with enhanced sensing performance. Sensors and Actuators B: Chemical, 2017, 238, 364-373.	7.8	118
9	High sensitive and fast formaldehyde gas sensor based on Ag-doped LaFeO3 nanofibers. Journal of Alloys and Compounds, 2017, 695, 1122-1127.	5.5	102
10	Preparation of Pd nanoparticle-decorated hollow SnO 2 nanofibers and their enhanced formaldehyde sensing properties. Journal of Alloys and Compounds, 2015, 651, 690-698.	5.5	99
11	Hierarchical Fe3O4@Co3O4 core–shell microspheres: Preparation and acetone sensing properties. Sensors and Actuators B: Chemical, 2014, 199, 346-353.	7.8	98
12	Semitransparent inverted polymer solar cells with MoO3/Ag/MoO3 as transparent electrode. Applied Physics Letters, 2009, 95, .	3.3	91
13	Electrospun nanofibers of p-type NiO/n-type ZnO heterojunction with different NiO content and its influence on trimethylamine sensing properties. Sensors and Actuators B: Chemical, 2015, 207, 90-96.	7.8	91
14	High performance humidity sensor based on metal organic framework MIL-101(Cr) nanoparticles. Journal of Alloys and Compounds, 2017, 695, 520-525.	5.5	82
15	Highly Efficient Semitransparent Polymer Solar Cells with Color Rendering Index Approaching 100 Using One-Dimensional Photonic Crystal. ACS Applied Materials & Interfaces, 2015, 7, 9920-9928.	8.0	81
16	A novel humidity sensor based on NH2-MIL-125(Ti) metal organic framework with high responsiveness. Journal of Nanoparticle Research, 2013, 15, 1.	1.9	76
17	Photocatalytic degradation of C.I. Acid Orange 52 in the presence of Zn-doped TiO2 prepared by a stearic acid gel method. Dyes and Pigments, 2008, 77, 204-209.	3.7	74
18	Self-sacrificing templated formation of Co3O4/ZnCo2O4 composite hollow nanostructures for highly sensitive detecting acetone vapor. Sensors and Actuators B: Chemical, 2018, 273, 1202-1210.	7.8	69

#	Article	IF	CITATIONS
19	Semitransparent polymer solar cells using V2O5/Ag/V2O5 as transparent anodes. Organic Electronics, 2011, 12, 1223-1226.	2.6	68
20	Performance improvement of TiO2â^•P3HT solar cells using CuPc as a sensitizer. Applied Physics Letters, 2008, 92, 073307.	3.3	67
21	Semitransparent Polymer Solar Cells with 5% Power Conversion Efficiency Using Photonic Crystal Reflector. ACS Applied Materials & Interfaces, 2014, 6, 599-605.	8.0	66
22	Ethanol sensing properties of LaCo Fe1â^'O3 nanoparticles: Effects of calcination temperature, Co-doping, and carbon nanotube-treatment. Sensors and Actuators B: Chemical, 2011, 155, 232-238.	7.8	65
23	Synthesis of Ni-doped α-MoO3 nanolamella and their improved gas sensing properties. Sensors and Actuators B: Chemical, 2017, 252, 757-763.	7.8	65
24	Self-Sacrificial Template-Driven LaFeO ₃ /α-Fe ₂ O ₃ Porous Nano-Octahedrons for Acetone Sensing. ACS Applied Nano Materials, 2018, 1, 4671-4681.	5.0	65
25	Surface state studies of TiO2 nanoparticles and photocatalytic degradation of methyl orange in aqueous TiO2 dispersions. Materials Chemistry and Physics, 2001, 69, 7-9.	4.0	64
26	Semitransparent inverted polymer solar cells using MoO3/Ag/WO3 as highly transparent anodes. Solar Energy Materials and Solar Cells, 2011, 95, 877-880.	6.2	64
27	Coordination Polymer-Derived Multishelled Mixed Ni–Co Oxide Microspheres for Robust and Selective Detection of Xylene. ACS Applied Materials & Interfaces, 2018, 10, 15314-15321.	8.0	64
28	Self-template derived ZnFe2O4 double-shell microspheres for chemresistive gas sensing. Sensors and Actuators B: Chemical, 2018, 265, 625-631.	7.8	64
29	Metal–organic framework-derived Co3O4/CoFe2O4 double-shelled nanocubes for selective detection of sub-ppm-level formaldehyde. Sensors and Actuators B: Chemical, 2019, 298, 126887.	7.8	62
30	Schottky Diode Ultraviolet Detector Based on \$ hbox{TiO}_{2}\$ Nanowire Array. IEEE Electron Device Letters, 2012, 33, 83-85.	3.9	60
31	Performance improvement of inverted polymer solar cells thermally evaporating nickel oxide as an anode buffer layer. Solar Energy Materials and Solar Cells, 2012, 98, 212-215.	6.2	60
32	Xylene gas sensor based on α-MoO ₃ /α-Fe ₂ O ₃ heterostructure with high response and low operating temperature. RSC Advances, 2015, 5, 39442-39448.	3.6	60
33	Gas Sensors Based on Metal Sulfide Zn _{1–<i>x</i>} Cd _{<i>x</i>} S Nanowires with Excellent Performance. ACS Applied Materials & Interfaces, 2015, 7, 20793-20800.	8.0	60
34	Synthesis and characterization of Cr-doped WO3 nanofibers for conductometric sensors with high xylene sensitivity. Sensors and Actuators B: Chemical, 2018, 265, 355-364.	7.8	60
35	Fe2O3 nanoparticles-decorated MoO3 nanobelts for enhanced chemiresistive gas sensing. Journal of Alloys and Compounds, 2019, 782, 672-678.	5.5	60
36	Effects of the optical microcavity on the performance of ITO-free polymer solar cells with WO3/Ag/WO3 transparent electrode. Solar Energy Materials and Solar Cells, 2012, 100, 226-230.	6.2	59

#	Article	IF	CITATIONS
37	Enhanced toluene sensing performance of gold-functionalized WO 3 ·H 2 O nanosheets. Sensors and Actuators B: Chemical, 2016, 223, 761-767.	7.8	58
38	Improved gas sensing properties of silver-functionalized ZnSnO ₃ hollow nanocubes. Inorganic Chemistry Frontiers, 2018, 5, 2123-2131.	6.0	56
39	V-doped In2O3 nanofibers for H2S detection at low temperature. Ceramics International, 2014, 40, 6685-6689.	4.8	55
40	Highly stabilized and rapid sensing acetone sensor based on Au nanoparticle-decorated flower-like ZnO microstructures. Journal of Alloys and Compounds, 2015, 650, 37-44.	5.5	55
41	Synergistically improved formaldehyde gas sensing properties of SnO2 microspheres by indium and palladium co-doping. Ceramics International, 2015, 41, 7329-7336.	4.8	55
42	Highly efficient rapid ethanol sensing based on In2â^'Ni O3 nanofibers. Sensors and Actuators B: Chemical, 2012, 166-167, 83-88.	7.8	54
43	The significant improvement for BTX (benzene, toluene and xylene) sensing performance based on Au-decorated hierarchical ZnO porous rose-like architectures. Sensors and Actuators B: Chemical, 2018, 262, 86-94.	7.8	53
44	A novel humidity sensor based on NaTaO3 nanocrystalline. Sensors and Actuators B: Chemical, 2012, 174, 485-489.	7.8	52
45	Highly Efficient Low-Bandgap Polymer Solar Cells with Solution-Processed and Annealing-Free Phosphomolybdic Acid as Hole-Transport Layers. ACS Applied Materials & Interfaces, 2015, 7, 5367-5372.	8.0	52
46	One-step synthesis and gas sensing properties of hierarchical Fe doped Co3O4 nanostructures. Journal of Alloys and Compounds, 2017, 723, 779-786.	5.5	52
47	High performance ultraviolet detector based on TiO2/ZnO heterojunction. Journal of Alloys and Compounds, 2015, 618, 551-554.	5.5	51
48	Improved gas sensing performance with Pd-doped WO3·H2O nanomaterials for the detection of xylene. Sensors and Actuators B: Chemical, 2017, 244, 837-848.	7.8	50
49	Metal–organic framework-derived ZnO/ZnCo2O4 microspheres modified by catalytic PdO nanoparticles for sub-ppm-level formaldehyde detection. Sensors and Actuators B: Chemical, 2020, 315, 128118.	7.8	50
50	Synthesis, characterization, and gas-sensing property for HCHO of Ag-doped In2O3 nanocrystalline powders. Materials Chemistry and Physics, 2009, 117, 489-493.	4.0	47
51	Oxygen vacancies dominated CuO@ZnFe2O4 yolk-shell microspheres for robust and selective detection of xylene. Sensors and Actuators B: Chemical, 2019, 295, 117-126.	7.8	47
52	Performance Improvement of Polymer Solar Cells by Surface-Energy-Induced Dual Plasmon Resonance. ACS Applied Materials & Interfaces, 2016, 8, 6183-6189.	8.0	46
53	Highly efficient and high transmittance semitransparent polymer solar cells with one-dimensional photonic crystals as distributed Bragg reflectors. Organic Electronics, 2014, 15, 470-477.	2.6	45
54	Preparation and Xyleneâ€Sensing Properties of Co ₃ O ₄ Nanofibers. International Journal of Applied Ceramic Technology, 2014, 11, 619-625.	2.1	45

#	Article	IF	CITATIONS
55	Surface Plasmon Resonance Enhanced Polymer Solar Cells by Thermally Evaporating Au into Buffer Layer. ACS Applied Materials & Interfaces, 2015, 7, 18866-18871.	8.0	45
56	Enhanced ethyl acetate sensing performance of Al-doped In2O3 microcubes. Sensors and Actuators B: Chemical, 2017, 253, 461-469.	7.8	45
57	Enhanced gas sensing properties for formaldehyde based on ZnO/Zn2SnO4 composites from one-step hydrothermal synthesis. Journal of Alloys and Compounds, 2021, 850, 156606.	5.5	45
58	Excellent gas sensing and optical properties of single-crystalline cadmium sulfide nanowires. RSC Advances, 2014, 4, 61691-61697.	3.6	44
59	Influences of different interdigital spacing on the performance of UV photodetectors based on ZnO nanofibers. Applied Surface Science, 2014, 307, 20-23.	6.1	44
60	Synthesis of au-decorated SnO2 crystallites with exposed (221) facets and their enhanced acetylene sensing properties. Sensors and Actuators B: Chemical, 2020, 307, 127629.	7.8	44
61	Visible-light photodetector with enhanced performance based on a ZnO@CdS heterostructure. Journal of Materials Chemistry C, 2015, 3, 2231-2236.	5.5	43
62	Xylene gas sensor based on Ni doped TiO ₂ bowl-like submicron particles with enhanced sensing performance. RSC Advances, 2015, 5, 28105-28110.	3.6	43
63	Preparation of three-dimensional Ce-doped Sn3O4 hierarchical microsphere and its application on formaldehyde gas sensor. Journal of Alloys and Compounds, 2017, 726, 1092-1100.	5.5	41
64	Semitransparent inverted polymer solar cells using MoO3/Ag/V2O5 as transparent anodes. Solar Energy Materials and Solar Cells, 2012, 97, 59-63.	6.2	40
65	Special nanostructure control of ethanol sensing characteristics based on Au@In ₂ O ₃ sensor with good selectivity and rapid response. RSC Advances, 2015, 5, 9884-9890.	3.6	40
66	Synthesis of SnO2 nano-dodecahedrons with high-energy facets and their sensing properties to SO2 at low temperature. Journal of Alloys and Compounds, 2017, 723, 595-601.	5.5	40
67	Hexagonal ZnO nanorings: synthesis, formation mechanism and trimethylamine sensing properties. RSC Advances, 2015, 5, 80561-80567.	3.6	38
68	Semitransparent polymer solar cells with one-dimensional (WO3/LiF)N photonic crystals. Applied Physics Letters, 2012, 101, .	3.3	37
69	HCHO sensing properties of Ag-doped In2O3 nanofibers synthesized by electrospinning. Materials Letters, 2009, 63, 1750-1753.	2.6	36
70	Ultraviolet photodetector with high internal gain enhanced by TiO_2/SrTiO_3 heterojunction. Optics Express, 2012, 20, 5936.	3.4	36
71	Simultaneous improvement in efficiency and transmittance of low bandgap semitransparent polymer solar cells with one-dimensional photonic crystals. Solar Energy Materials and Solar Cells, 2013, 117, 198-202.	6.2	36
72	Synthesis of hierarchical 3D porous ZnO microspheres decorated by ultra-small Au nanoparticles and its highly enhanced acetylene gas sensing ability. Journal of Alloys and Compounds, 2018, 731, 1029-1036.	5.5	36

#	Article	IF	CITATIONS
73	Fe3O4–NiO core–shell composites: Hydrothermal synthesis and toluene sensing properties. Materials Letters, 2014, 132, 167-170.	2.6	35
74	Humidity sensing properties of FeCl3-NH2-MIL-125(Ti) composites. Sensors and Actuators B: Chemical, 2014, 201, 281-285.	7.8	34
75	Xylene sensor based on α-MoO ₃ nanobelts with fast response and low operating temperature. RSC Advances, 2015, 5, 18655-18659.	3.6	33
76	An easily prepared carbon quantum dots and employment for inverted organic photovoltaic devices. Chemical Engineering Journal, 2017, 315, 621-629.	12.7	33
77	Open-circuit voltage enhancement of inverted polymer bulk heterojunction solar cells by doping NaYF4 nanoparticles/PVP composites. Journal of Materials Chemistry, 2012, 22, 22382.	6.7	32
78	A new type of acetylene gas sensor based on a hollow heterostructure. RSC Advances, 2015, 5, 61521-61527.	3.6	32
79	Unique Gold Nanorods Embedded Active Layer Enabling Strong Plasmonic Effect To Improve the Performance of Polymer Photovoltaic Devices. Journal of Physical Chemistry C, 2016, 120, 6198-6205.	3.1	32
80	Annealing-Free ZnO:PEI Composite Cathode Interfacial Layer for Efficient Organic Solar Cells. ACS Photonics, 2017, 4, 2952-2958.	6.6	32
81	Tailoring Spatial Distribution of the Optical Field Intensity in Semitransparent Inverted Organic Solar Cells. Journal of Physical Chemistry C, 2011, 115, 12611-12615.	3.1	31
82	TiO2 ultraviolet detector based on LaAlO3 substrate with low dark current. Journal of Alloys and Compounds, 2013, 580, 614-617.	5.5	31
83	One-step synthesis and the enhanced xylene-sensing properties of Fe-doped MoO ₃ nanobelts. RSC Advances, 2016, 6, 106364-106369.	3.6	31
84	Engineering Co3+ cations in Co3O4 multishelled microspheres by Mn doping: The roles of Co3+ and oxygen species for sensitive xylene detection. Sensors and Actuators B: Chemical, 2020, 308, 127651.	7.8	31
85	Enhanced Electron Extraction Capability of Polymer Solar Cells via Employing Electrostatically Self-Assembled Molecule on Cathode Interfacial Layer. ACS Applied Materials & Interfaces, 2016, 8, 8224-8231.	8.0	29
86	The effects of Zr-doping on improving the sensitivity and selectivity of a one-dimensional α-MoO ₃ -based xylene gas sensor. Inorganic Chemistry Frontiers, 2020, 7, 1704-1712.	6.0	29
87	Decreased Charge Transport Barrier and Recombination of Organic Solar Cells by Constructing Interfacial Nanojunction with Annealing-Free ZnO and Al Layers. ACS Applied Materials & Interfaces, 2017, 9, 22068-22075.	8.0	28
88	An organic–inorganic hybrid UV photodetector based on a TiO2 nanobowl array with high spectrum selectivity. RSC Advances, 2013, 3, 21413.	3.6	27
89	Facile fabrication of NaTaO3 film and its photoelectric properties. Journal of Alloys and Compounds, 2014, 602, 322-325.	5.5	27
90	Template-free synthesis of Cu ₂ O–Co ₃ O ₄ core–shell composites and their application in gas sensing. RSC Advances, 2014, 4, 24211-24216.	3.6	27

Shengping Ruan

#	Article	IF	CITATIONS
91	Ultraviolet detector based on TiO2 nanowire array–polymer hybrids with low dark current. Journal of Alloys and Compounds, 2015, 618, 233-235.	5.5	27
92	Trappedâ€Electronâ€Induced Hole Injection in Perovskite Photodetector with Controllable Gain. Advanced Optical Materials, 2018, 6, 1701189.	7.3	27
93	Synthesis of CuO–CdS composite nanowires and their ultrasensitive ethanol sensing properties. Inorganic Chemistry Frontiers, 2019, 6, 238-247.	6.0	27
94	Metal-organic framework derived core-shell PrFeO3-functionalized α-Fe2O3 nano-octahedrons as high performance ethyl acetate sensors. Sensors and Actuators B: Chemical, 2019, 297, 126738.	7.8	27
95	The role of Ag nanoparticles in inverted polymer solar cells: Surface plasmon resonance and backscattering centers. Applied Physics Letters, 2013, 102, .	3.3	26
96	Effects of growth substrates on the morphologies of TiO2 nanowire arrays and the performance of assembled UV detectors. Applied Surface Science, 2014, 315, 55-58.	6.1	26
97	Humidity sensing properties of MoO3-NiO nanocomposite materials. Ceramics International, 2015, 41, 4348-4353.	4.8	26
98	Hierarchical Co3O4@NiMoO4 core-shell nanowires for chemiresistive sensing of xylene vapor. Mikrochimica Acta, 2019, 186, 222.	5.0	26
99	Multiple microwave frequencies measurement based on stimulated Brillouin scattering with improved measurement range. Optics Express, 2013, 21, 31740.	3.4	25
100	Enhanced performance of a TiO ₂ ultraviolet detector modified with graphene oxide. RSC Advances, 2015, 5, 83795-83800.	3.6	25
101	The Performance Enhancement of Polymer Solar Cells by Introducing Cadmium-Free Quantum Dots. Journal of Physical Chemistry C, 2015, 119, 26747-26752.	3.1	25
102	Boosted Electron Transport and Enlarged Built-In Potential by Eliminating the Interface Barrier in Organic Solar Cells. ACS Applied Materials & Interfaces, 2017, 9, 8830-8837.	8.0	25
103	Light harvesting enhancement toward low IPCE region of semitransparent polymer solar cells via one-dimensional photonic crystal reflectors. Solar Energy Materials and Solar Cells, 2014, 127, 27-32.	6.2	24
104	Hydrothermal synthesis and enhanced xylene-sensing properties of pompon-like Cr-doped Co ₃ O ₄ hierarchical nanostructures. RSC Advances, 2016, 6, 22889-22895.	3.6	24
105	<pre>\$hbox{Zr}_{0.27}hbox{Ti}_{0.73}hbox{O}_{2}\$-Based MSM Ultraviolet Detectors With Pt Electrodes. IEEE Electron Device Letters, 2011, 32, 653-655.</pre>	3.9	23
106	Low temperature operating In2â^'xNixO3 sensors with high response and good selectivity for NO2 gas. Journal of Alloys and Compounds, 2013, 581, 653-658.	5.5	23
107	High response solar-blind ultraviolet photodetector based on Zr0.5Ti0.5O2 film. Applied Surface Science, 2013, 268, 312-316.	6.1	23
108	Performance improvement of inverted polymer solar cells by doping Au nanoparticles into TiO2 cathode buffer layer. Applied Physics Letters, 2013, 103, .	3.3	23

#	Article	IF	CITATIONS
109	Highly efficient ITO-free polymer solar cells based on metal resonant microcavity using WO3/Au/WO3 as transparent electrodes. Organic Electronics, 2014, 15, 1545-1551.	2.6	23
110	The preparation of Cr ₂ O ₃ @WO ₃ hierarchical nanostructures and their application in the detection of volatile organic compounds (VOCs). RSC Advances, 2015, 5, 61528-61534.	3.6	23
111	Synthesis and enhanced gas sensing properties of Au-nanoparticle decorated CdS nanowires. RSC Advances, 2016, 6, 70907-70912.	3.6	23
112	G-C3N4/In2O3 composite for effective formaldehyde detection. Sensors and Actuators B: Chemical, 2022, 358, 131414.	7.8	23
113	Organics filled one-dimensional TiO ₂ nanowires array ultraviolet detector with enhanced photo-conductivity and dark-resistivity. Nanoscale, 2017, 9, 9095-9103.	5.6	22
114	Improving the charge carrier transport of organic solar cells by incorporating a deep energy level molecule. Physical Chemistry Chemical Physics, 2017, 19, 245-250.	2.8	22
115	Novel ultraviolet photodetector with ultrahigh photosensitivity employing SILAR-deposited ZnS film on MgZnO. Journal of Alloys and Compounds, 2020, 832, 155022.	5.5	22
116	Electrospun <scp><scp>ZnO</scp> </scp> Nanofibersâ€Based Ultraviolet Detector with High Responsivity. Journal of the American Ceramic Society, 2013, 96, 3183-3187.	3.8	21
117	An ultrawide tunable range single passband microwave photonic filter based on stimulated Brillouin scattering. Optics Express, 2013, 21, 2718.	3.4	21
118	Humidity sensor based on AlPO4-5 zeolite with high responsivity and its sensing mechanism. Sensors and Actuators B: Chemical, 2015, 212, 242-247.	7.8	20
119	Improving the efficiency of inverted polymer solar cells by introducing inorganic dopants. Physical Chemistry Chemical Physics, 2015, 17, 7960-7965.	2.8	20
120	Improved Power Conversion Efficiency of Inverted Organic Solar Cells by Incorporating Au Nanorods into Active Layer. ACS Applied Materials & Interfaces, 2015, 7, 15848-15854.	8.0	20
121	Synthesis and highly enhanced acetylene sensing properties of Au nanoparticle-decorated hexagonal ZnO nanorings. RSC Advances, 2015, 5, 87132-87138.	3.6	20
122	High performance ultraviolet detector based on SrTiO3/TiO2 heterostructure fabricated by two steps in situ hydrothermal method. Journal of Alloys and Compounds, 2015, 650, 97-101.	5.5	20
123	The effect of self-depleting in UV photodetector based on simultaneously fabricated TiO ₂ /NiO pn heterojunction and Ni/Au composite electrode. Nanotechnology, 2017, 28, 365505.	2.6	20
124	Construction of p-n heterojunctions by modifying MOF-derived α-Fe2O3 with partially covered cobalt tungstate for high-performance ethyl acetate detection. Sensors and Actuators B: Chemical, 2021, 344, 130129.	7.8	20
125	Combining plasmonic trap filling and optical backscattering for highly efficient third generation solar cells. Journal of Materials Chemistry A, 2017, 5, 3995-4002.	10.3	19
126	<pre>\$hbox{Zr}_{x}hbox{Ti}_{1 - x}hbox{O}_{2}*Based Ultraviolet Detectors Series. IEEE Electron Device Letters, 2011, 32, 934-936.</pre>	3.9	18

8

#	Article	IF	CITATIONS
127	Synthesis and photovoltaic properties of dithieno[3,2-b:2′,3′-d]silole-based conjugated copolymers. Journal of Materials Chemistry A, 2015, 3, 13794-13800.	10.3	18
128	Small molecules based on tetrazine unit for efficient performance solution-processed organic solar cells. Solar Energy Materials and Solar Cells, 2016, 155, 30-37.	6.2	18
129	Suppressing TiO ₂ /Perovskite Interfacial Electron Trapping in Perovskite Solar Cell for Efficient Charge Extraction and Improved Device Performance. ACS Sustainable Chemistry and Engineering, 2018, 6, 11295-11302.	6.7	18
130	Effects of surface self-assembled NH4+ on the performance of TiO2-based ultraviolet photodetectors. Journal of Alloys and Compounds, 2014, 601, 104-107.	5.5	17
131	Versatile dual organic interface layer for performance enhancement of polymer solar cells. Journal of Power Sources, 2016, 333, 99-106.	7.8	17
132	Passivation agent with dipole moment for surface modification towards efficient and stable perovskite solar cells. Journal of Energy Chemistry, 2022, 64, 55-61.	12.9	17
133	Schottky barrier characteristics and internal gain mechanism of TiO ₂ UV detectors. Applied Optics, 2012, 51, 894.	1.8	16
134	Humidity sensing properties of SrTiO ₃ nanospheres with high sensitivity and rapid response. RSC Advances, 2015, 5, 22879-22883.	3.6	16
135	Efficiency Improvement of Organic Solar Cells via Introducing Combined Anode Buffer Layer To Facilitate Hole Extraction. Journal of Physical Chemistry C, 2016, 120, 13954-13962.	3.1	16
136	Delicate Energy-Level Adjustment and Interfacial Defect Passivation of ZnO Electron Transport Layers in Organic Solar Cells by Constructing ZnO/In Nanojunctions. Journal of Physical Chemistry C, 2019, 123, 16546-16555.	3.1	16
137	Short-circuit current density improvement of inverted polymer solar cells using PbPc to enhance photon absorption over 600 nm. Solar Energy Materials and Solar Cells, 2010, 94, 2451-2454.	6.2	15
138	Efficiency enhancement of inverted organic solar cells by introducing PFDTBT quantum dots into PCDTBT:PC71BM active layer. Organic Electronics, 2014, 15, 2632-2638.	2.6	15
139	Ultrahigh responsivity UV detector based on TiO2/Pt-doped TiO2 multilayer nanofilms. Journal of Alloys and Compounds, 2014, 616, 155-158.	5.5	15
140	Performance improvement of inverted polymer solar cells thermally evaporating CuI as an anode buffer layer. Synthetic Metals, 2014, 198, 1-5.	3.9	15
141	Low-temperature synthesis of WO3 nanolamella and their sensing properties for xylene. RSC Advances, 2015, 5, 85598-85605.	3.6	15
142	UV detector based on an FTO/TiO ₂ /MoO ₃ heterojunction with a potential well trapping electrons in the dark. Nanotechnology, 2019, 30, 465501.	2.6	15
143	Three dimensions sphere formaldehyde nanosensor applications: preparation and sensing properties. RSC Advances, 2015, 5, 50336-50343.	3.6	14
144	Improved color rendering index of low band gap semi-transparent polymer solar cells using one-dimensional photonic crystals. RSC Advances, 2015, 5, 54638-54644.	3.6	14

#	Article	IF	CITATIONS
145	Synthesis of sea urchin-like microsphere of CdS and its gas sensing properties. Materials Science and Engineering B: Solid-State Materials for Advanced Technology, 2019, 243, 206-213.	3.5	14
146	Mesoporous titanium niobium nitrides supported Pt nanoparticles for highly selective and sensitive formaldehyde sensing. Journal of Materials Chemistry A, 2021, 9, 19840-19846.	10.3	14
147	Influences of surface capping with electrostatically self-assembled PEI on the photoresponse of a TiO2 thin film. Chemical Communications, 2013, 49, 6328.	4.1	13
148	Improved Efficiency in Dithieno[3,2-b:2′,3′-d]silole-Based Polymer Solar Cells by the Insertion of ZnO Optical Spacer. Journal of Physical Chemistry C, 2015, 119, 20817-20822.	3.1	13
149	Polyelectrolyte interlayers with a broad processing window for high efficiency inverted organic solar cells towards mass production. Journal of Materials Chemistry A, 2018, 6, 17662-17670.	10.3	13
150	Built-in electric field promotes photoexcitation separation and depletion of most carriers in TiO ₂ :C UV detectors. Nanotechnology, 2019, 30, 295502.	2.6	13
151	Molecular Doping Inhibits Charge Trapping in Low-Temperature-Processed ZnO toward Flexible Organic Solar Cells. ACS Applied Materials & Interfaces, 2021, 13, 14423-14432.	8.0	13
152	The role of Au nanorods in highly efficient inverted low bandgap polymer solar cells. Applied Physics Letters, 2014, 105, 223305.	3.3	12
153	Facilitated extrinsic majority carrier depletion and photogenerated exciton dissociation in an an annealing-free ZnO:C photodetector. Nanoscale, 2018, 10, 6459-6466.	5.6	12
154	Enhanced Electronic Quality of Perovskite via a Novel C ₆₀ o-Quinodimethane Bisadducts toward Efficient and Stable Perovskite Solar Cells. ACS Sustainable Chemistry and Engineering, 2019, 7, 8579-8586.	6.7	12
155	Analysis and design of tunable wideband microwave photonics phase shifter based on Fabry–Perot cavity and Bragg mirrors in silicon-on-insulator waveguide. Applied Optics, 2010, 49, 2391.	2.1	11
156	Role of solution-processed V2O5 in P3HT:PCBM based inverted polymer solar cells. Synthetic Metals, 2013, 170, 7-10.	3.9	10
157	Application of Solution-Processed V ₂ O ₅ in Inverted Polymer Solar Cells Based on Fluorine-Doped Tin Oxide Substrate. Journal of Nanoscience and Nanotechnology, 2014, 14, 4214-4217.	0.9	10
158	Performance enhancement of organic photovoltaic devices enabled by Au nanoarrows inducing surface plasmonic resonance effect. Physical Chemistry Chemical Physics, 2016, 18, 24285-24289.	2.8	10
159	Enhanced Photovoltaic Performance of Tetrazine-Based Small Molecules with Conjugated Side Chains. ACS Sustainable Chemistry and Engineering, 2017, 5, 8684-8692.	6.7	10
160	Enhanced electron extraction capability of polymer solar cells via modifying the cathode buffer layer with inorganic quantum dots. Physical Chemistry Chemical Physics, 2016, 18, 11435-11442.	2.8	9
161	Fabrication of Sm-doped porous In2O3 nanotubes and their excellent formaldehyde-sensing properties. Journal of Materials Science: Materials in Electronics, 2016, 27, 9870-9876.	2.2	9
162	Highly efficient polymer solar cells based on low-temperature processed ZnO: application of a bifunctional Au@CNTs nanocomposite. Journal of Materials Chemistry C, 2019, 7, 2676-2685.	5.5	9

#	Article	IF	CITATIONS
163	Mesoporous Ti0.5Cr0.5N for trace H2S detection with excellent long-term stability. Journal of Hazardous Materials, 2022, 423, 127193.	12.4	9
164	Synthesis and gas sensing properties of β-Fe2O3 derived from Fe/Ga bimetallic organic framework. Journal of Alloys and Compounds, 2022, 921, 166193.	5.5	9
165	Effect of the fluorinated groups on nematic liquid crystal alignment on monomer crosslinked film. Thin Solid Films, 2004, 466, 326-330.	1.8	8
166	Performance Improvement of Low-Band-Gap Polymer Solar Cells by Optical Microcavity Effect. IEEE Electron Device Letters, 2013, 34, 87-89.	3.9	8
167	Enhancing the light-harvesting and charge transport properties of polymer solar cells by embedding NaLuF ₄ :Yb,Tm nanorods. RSC Advances, 2015, 5, 32891-32896.	3.6	8
168	Optimization of PDTS-DTffBT-Based Solar Cell Performance through Control of Polymer Molecular Weight. Journal of Physical Chemistry C, 2016, 120, 19513-19520.	3.1	8
169	Applications for rapid formaldehyde nanoreactor with hierarchical and spherical structure. Sensors and Actuators B: Chemical, 2016, 227, 475-481.	7.8	8
170	Interface passivation and electron transport improvement of polymer solar cells through embedding a polyfluorene layer. Physical Chemistry Chemical Physics, 2017, 19, 15207-15214.	2.8	8
171	Incorporating deep electron traps into perovskite devices: towards high efficiency solar cells and fast photodetectors. Journal of Materials Chemistry A, 2018, 6, 21039-21046.	10.3	8
172	Using Ligand Engineering to Produce Efficient and Stable Pb–Sn Perovskite Solar Cells with Antioxidative 2D Capping Layers. ACS Applied Materials & Interfaces, 2022, 14, 14729-14738.	8.0	8
173	Design and fabrication of slant-counter electrodes for optical switches. Microwave and Optical Technology Letters, 2004, 41, 273-275.	1.4	7
174	Preparation and NO ₂ Sensing Properties of the Ni-Doped In ₂ O ₃ Nanofibers. Integrated Ferroelectrics, 2012, 138, 71-76.	0.7	7
175	Mechanism of Polyfluorene Interlayer in Ultraviolet Photodetector: Barrier-Blocking Electron Transport and Light-Inducing Hole Injection. Journal of Physical Chemistry C, 2016, 120, 26103-26109.	3.1	7
176	Design of a vector-sum integrated microwave photonic phase shifter in silicon-on-insulator waveguides. Applied Optics, 2011, 50, 2523.	2.1	6
177	Photoelectric Properties of TiO2–ZrO2 Thin Films Prepared by Sol–Gel Method. Journal of Nanoscience and Nanotechnology, 2011, 11, 10003-10006.	0.9	6
178	Efficient Semitransparent Inverted Polymer Solar Cells With the Anode of Tunable Incident Light Transmittance. IEEE Electron Device Letters, 2012, 33, 1027-1029.	3.9	6
179	Photoelectron Properties of Nanocrystalline <scp><scp>TiO</scp>2 Films Prepared by a Powerful Hydrothermal Technique. Journal of the American Ceramic Society, 2012, 95, 1980-1984.</scp>	3.8	6
180	\${m NaTaO}_{3}\$-Based Ultraviolet Photodetector With Capacitive Efficacy. IEEE Electron Device Letters, 2013, 34, 1539-1541.	3.9	6

#	Article	IF	CITATIONS
181	Unraveling the effect of polymer dots doping in inverted low bandgap organic solar cells. Physical Chemistry Chemical Physics, 2015, 17, 16086-16091.	2.8	6
182	Research of dual-band microwave photonic filter for WLAN based on optical frequency comb. Applied Optics, 2016, 55, 5520.	2.1	6
183	The role of polymer dots on efficiency enhancement of organic solar cells: Improving charge transport property. Optics Communications, 2017, 395, 127-132.	2.1	6
184	Orienting the Microstructure Evolution of Copper Phthalocyanine as an Anode Interlayer in Inverted Polymer Solar Cells for High Performance. ACS Applied Materials & Interfaces, 2017, 9, 32044-32053.	8.0	6
185	Employing Pentacene To Balance the Charge Transport in Inverted Organic Solar Cells. Journal of Physical Chemistry C, 2018, 122, 17110-17117.	3.1	6
186	Preparation and Ethanol Sensing Properties of In ₂ O ₃ Nanotubes. Journal of Nanoscience and Nanotechnology, 2014, 14, 3653-3657.	0.9	5
187	Solar-Blind Photodetector Based on LaAlO ₃ with Low Dark Current. Journal of Nanoscience and Nanotechnology, 2014, 14, 3827-3830.	0.9	5
188	Design of thermo-optic tunable optical filter based on Si/Air DBR and polymer Fabry–Perot microcavity in SOI. Optik, 2014, 125, 2885-2890.	2.9	5
189	An organosilane self-assembled monolayer incorporated into polymer solar cells enabling interfacial coherence to improve charge transport. Physical Chemistry Chemical Physics, 2016, 18, 16005-16012.	2.8	5
190	Modulated charge transport characteristics in solution-processed UV photodetector by incorporating localized built-in electric field. Journal of Alloys and Compounds, 2019, 774, 887-895.	5.5	5
191	Ultraviolet Detector Based on \$hbox{SrZr}_{0.1} hbox{Ti}_{0.9}hbox{O}_{3}\$ Film. IEEE Electron Device Letters, 2013, 34, 420-422.	3.9	4
192	Humidity sensing properties of CeO2–NiO nanocomposite materials. Journal of Materials Science: Materials in Electronics, 2015, 26, 3083-3089.	2.2	4
193	Single passband microwave photonic filter with high selectivity and large tunable range. Optical and Quantum Electronics, 2015, 47, 1589-1597.	3.3	4
194	The operation mechanism of poly(9,9-dioctylfluorenyl-2,7-diyl) dots in high efficiency polymer solar cells. Applied Physics Letters, 2015, 106, .	3.3	4
195	Optically tunable frequency-sextupling optoelectronic oscillator based on Brillouin gain-loss compensation and carrier phase-shifted double sideband modulation. Optical and Quantum Electronics, 2015, 47, 3455-3465.	3.3	4
196	Bandwidth reconfigurable microwave photonic filter based on stimulated Brillouin scattering. Optical Fiber Technology, 2015, 21, 187-192.	2.7	4
197	Employing inorganic/organic hybrid interface layer to improve electron transfer for inverted polymer solar cells. Electrochimica Acta, 2016, 210, 874-879.	5.2	4
198	Dual Roles of the Fullerene Interlayer on Light Harvesting and Electron Transfer for Highly Efficient Polymer Solar Cells. Journal of Physical Chemistry C, 2017, 121, 8722-8730.	3.1	4

#	Article	IF	CITATIONS
199	Excellent Gas Sensing of CdS Nanowires Decorated with Ag Nanoparticles. Journal of Nanoscience and Nanotechnology, 2019, 19, 7083-7088.	0.9	4
200	Surface oxidation for enhancing the hydrogen evolution reaction of metal nitrides: a theoretical study on vanadium nitride. Materials Advances, 0, , .	5.4	4
201	Sodium Titanate Nanorod Moisture Sensor and Its Sensing Mechanism. IEEE Electron Device Letters, 2013, 34, 1424-1426.	3.9	3
202	Photovoltaic ultraviolet detectors based on Zr ₀₀₄ Ti ₀₉₆ O ₂ solid solution nanowire arrays. Applied Optics, 2013, 52, 750.	1.8	3
203	Using a facile processing method to facilitate charge extraction for polymer solar cells. Journal of Materials Chemistry C, 2018, 6, 11045-11051.	5.5	3
204	Preparation of polymer liquid crystal material for use in the variable optical attenuator. , 2005, 5623, 541.		2
205	Fabrication of TiO <inf>2</inf> Schottky barrier diodes by RF magnetron sputtering. , 2008, , .		2
206	Research on MEMS acceleration sensor detection circuit based on adaptive filter. , 2009, , .		2
207	Performance study of microwave photonic phase shifter based on vector-sum technique. Optik, 2013, 124, 6140-6145.	2.9	2
208	Photovoltaic Properties of Zr _{<i>x</i>} Ti _{1–<i>x</i>} O _{2& Solid Solution Nanowire Arrays. Journal of Nanoscience and Nanotechnology, 2014, 14, 3731-3734.}	lt; /S.l dB&g	t; 2
209	Efficiency Improvement of Inverted Organic Solar Cells via Introducing a Series of Polyfluorene Dots in Electron Transport Layer. Journal of Physical Chemistry C, 2015, 119, 16462-16467.	3.1	2
210	A PFTBT modified visible-blind ultraviolet photodetector with a narrow detecting range and high responsivity. Nanotechnology, 2018, 29, 465501.	2.6	2
211	The Photocurrent Improvement of Inverted Polymer Solar Cells Using ZnPc to Extend Light Absorption Range. , 2011, , .		1
212	The Study of Transmission Characteristics of a 17×17 All Fluorinated Polyimide Arrayed Waveguide Grating Multiplexer. , 2011, , .		1
213	Photonic generation of ultrawideband doublet pulse based on cross-absorption modulation in an electroabsorption modulator. , 2011, , .		1
214	Zr0.05Ti0.95O2-Nanowire-Based Ultraviolet Photodetector with Self-Powered Properties. Applied Physics Express, 2013, 6, 062002.	2.4	1
215	The Short Circuit Current Improvement in P3HT:PCBM Based Polymer Solar Cell by Introducing PSBTBT as Additional Electron Donor. Journal of Nanoscience and Nanotechnology, 2014, 14, 3446-3449.	0.9	1
216	The study of an ultrawide tunable range single passband microwave photonic notch filter. Optik, 2015, 126, 2512-2517.	2.9	1

#	Article	IF	CITATIONS
217	Improved performance of inverted polymer solar cells using Cd 2 SSe/ZnS quantum dots. Materials Letters, 2017, 188, 244-247.	2.6	1
218	New method of optical variable attenuator with polymer-network liquid crystals. , 2004, , .		0
219	Transparent ITO electrode in the polymer network liquid crystal variable optical attenuator. , 2004, 5280, 397.		0
220	Affect on the UV polymerization condition of polymer liquid crystal materials for variable optical attenuator. , 2008, , .		0
221	Study on PDLC films for variable optical attenuation in optical communication. , 2011, , .		0
222	MSM Ultraviolet Detectors Based on Zr _{0.1} Ti _{0.9} O ₂ Solid Solution. Integrated Ferroelectrics, 2012, 138, 94-99.	0.7	0
223	TiO2 Ultraviolet Detectors with Sandwich Structure. Integrated Ferroelectrics, 2012, 135, 138-143.	0.7	0
224	Modelling of Charge Carrier Mobility Effect on Organic Bulk Heterojunction Solar Cells. Integrated Ferroelectrics, 2012, 138, 38-43.	0.7	0
225	Analysis of plasma waves resonant detection for terahertz radiation in high mobility field effect transistor. Optik, 2013, 124, 6408-6410.	2.9	0
226	The Role of Fe ₃ O ₄ Nanocrystal Film in Bilayer-Heterojunction CuPc/C ₆₀ Solar Cells. Journal of Nanoscience and Nanotechnology, 2014, 14, 3623-3626.	0.9	0
227	Increasing the fill factor of inverted polymer bulk heterojunction solar cells by doping PVP modified NaYF4nanoparticles. Integrated Ferroelectrics, 2017, 180, 168-174.	0.7	Ο